

# Estimation of force coefficients for normal forces on bilge keels and skin friction roll damping of ships by CFD simulations

Sven Wassermann\*, *Hamburg University of Technology*, sven.wassermann@tuhh.de

Gregor Krambs, *Hamburg University of Technology*, gregor.krambs@tuhh.de

Moustafa Abdel-Maksoud, *Hamburg University of Technology*, m.abdel-maksoud@tuhh.de

## ABSTRACT

A finite-volume method (FVM) is used to simulate the roll motion of an ellipsoid equipped with wall-bounded flat plates with and without forward speed. Due to the circular form and a fixed roll axis of the simulated ellipsoid, only normal forces act on the plates. The normal force component in phase with the roll velocity over a harmonic roll period is estimated. The roll period, amplitude and the plate dimension are varied. The simulation results are compared with results of different model test techniques. The focus is set on modeling a simple definition for the normal force coefficient based on the Keulegan-Carpenter number ( $KC$ ). Compared to Ikeda's method, an improved definition which considers a larger range of  $KC$  numbers is formulated.

To transfer roll damping results from model scale into full scale, the frictional roll damping component of different ships is investigated. FVM simulations of the roll motion with various scales are carried out. A simple extrapolation procedure based on Kato's approach is developed.

**Keywords:** roll damping, force coefficient method, Ikeda's method, bilge keels, skin friction roll damping, scale effects

\*corresponding author, name at birth: Sven Handschel

## 1. INTRODUCTION

### Normal Forces on Bilge Keels

The roll motion of ships in waves is weakly damped by wave radiation. Simple roll damping devices such as bilge keels (BK) have the advantage to damp ships with and without forward speed in all weather conditions. Bilge keel constructions of a width up to 450mm with shipbuilding profiles were the industry practice in the last decades. In the mean time, the ship beam grew which led to large ratio of roll radius ( $r_{BK}$ ) to bilge keel width ( $b_{BK}$ ), see Table 1.

The authors have found two different common techniques which are used to measure normal

| $KC$ | Examples         | $r_{BK}/b_{BK}$ | $\varphi_a$ [deg] |
|------|------------------|-----------------|-------------------|
| 200  | plate in a tank  | 121.5           | 30                |
| 100  | BK on ULCC       | 72.75           | 25                |
| 25   | BK on RoPax      | 45.5            | 10                |
| 2    | keel on lifeboat | 7.4             | 5                 |
| 0.3  | plate at a buoy  | 1.2             | 5                 |

**Table 1:** Examples of wall bounded flat plates, e.g. bilge keels, for low and high  $KC$ -numbers ( $r_{BK}$ -roll radius,  $b_{BK}$ -plate width,  $\varphi_a$ -roll amplitude).

forces on wall bounded plates: (A) measurement of ellipsoid models in towing tanks and (B) force measurements in U-Tanks, see Figure 1. Ikeda et al. (1976) and Fujino et al. (1979) used an ellipsoid, respectively a spindle-like body to determine the drag force coefficient  $c_E$ . Sarpkaya and O'Keefe (1996) measured the force coefficient  $c_E$  for different plate dimensions in a U-Tank. The force coefficients for different  $KC$  numbers estimated by the mentioned experimental techniques are compared in Figure 2. Additionally the approximation function which is used in Ikeda's method and Ikeda's given range of validity,

$$c_{E,Ikeda} = \frac{22.5}{KC} + 2.4 \quad \text{for } 4 < KC < 20 \quad (1)$$

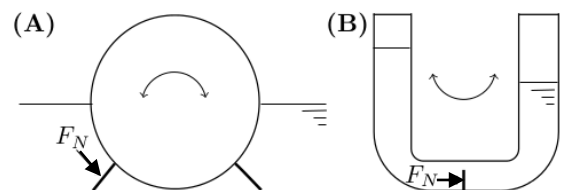


**Figure 1:** Techniques to measure the normal force on flat plates  $F_N$ : (A) - periodical rolling ellipsoid body in towing tank, (B) U-Tank with periodical flow.

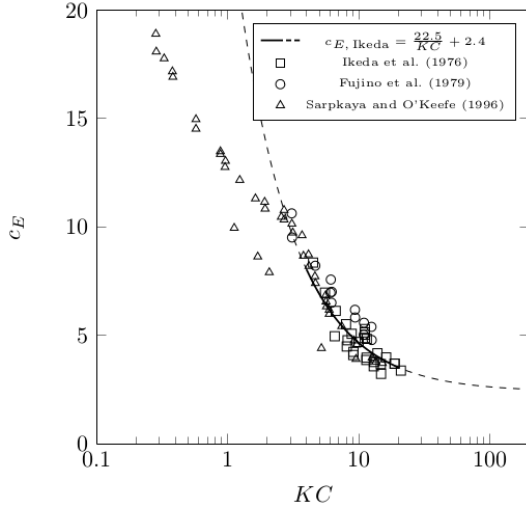


**Figure 2: Force coefficients of normal forces on BK - Comparison of experimental measurement values and Eq. 1 (Ikeda's Method)**

with

$$KC = \pi \frac{r_{BK} \varphi_a}{b_{BK}}, \quad (2)$$

is plotted in this Figure. It can be clearly seen that

1. no experiences exist for  $KC > 20$  and
2. Eq. (1) does not fit for  $KC < 3$ .

The paper presents a FVM simulation approach to estimate force coefficients  $c_E$  for  $KC$ -values between 0.5 and 100. Eq. (1) will be improved.

### Skin Friction Roll Damping

The skin friction roll damping is the smallest damping component and is mainly influenced by flow phenomena which depend on Reynolds number. Nevertheless, if Froude similarity is used to extrapolate the damping moment to full scale, a large scale factor can overestimate the total roll damping significantly. An extrapolation error of 5% and more is typical for large scale factors, see ITTC (2011). Figure 3 shows the influence of skin friction damping on total roll damping for the benchmarking Duisburg Test Case (DTC, el Moctar et al., 2012) container ship. The result given in Figure 3 is based on the later presented new approach.

The skin friction roll damping moment  $M_F(\dot{\varphi})$  was focused on in previous studies. Especially the estimation approach of Ikeda (1978), based on results of Kato (1958) for  $M_{F0e}$  and Tamiya (1972) for forward speed correction, became common practice and is recommended by the ITTC (2011).

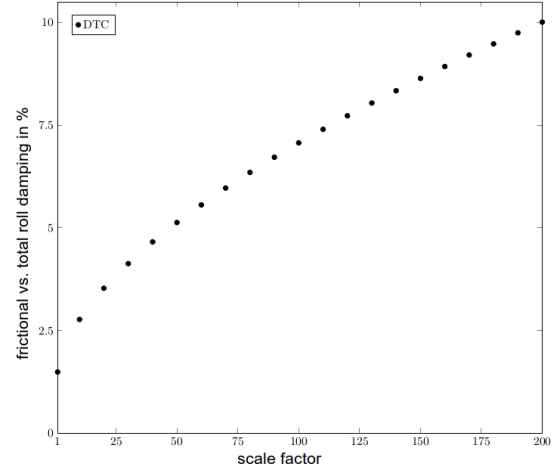


**Figure 3: Influence of skin friction damping on total roll damping for Duisburg Test Case (DTC)**

For a harmonic full roll cycle, it will be assumed that the roll damping moment can be approximated by a linear coefficient:  $M_F(\dot{\varphi}) = M_{Fe} \dot{\varphi}$ . The approach is based on the forward velocity  $U$  of the ship, the ship length  $L_{WL}$  at waterline, the roll frequency  $\omega$ , the kinetic viscosity  $\nu$  and the wetted surface of the ship  $S$ :

$$\frac{M_{Fe, Ikeda}}{M_{F0e}} = 1 + 0.653KC_L = 1 + 4.1 \frac{U}{\omega L_{WL}}, \quad (3)$$

$$M_{F0e} = 0.787 \rho S \bar{r}^2 \sqrt{\omega \nu} \left[ 1 + 0.00814 \left( \frac{\bar{r}^2 \varphi_a^2 \omega}{\nu} \right)^{0.386} \right]. \quad (4)$$

To estimate an equivalent roll radius  $\bar{r}$ , Kato (1958) used the following empirical method ( $\overline{OG}$ -distance from origin at waterline to center of gravity, coordinate system positive downwards):

$$\bar{r} = \frac{1}{\pi} \left( [0.887 + 0.145C_B] \frac{S}{L_{WL}} - 2\overline{OG} \right). \quad (5)$$

Based on FVM simulations of 39 test cases of three modern monohull ship forms, a database of skin friction coefficients was generated. A comparison with Ikeda's method shows an averaged deviation of the maximum frictional moment  $M_{F,max}$  formulated as mean squared error (MSE) of 1.75. Based on Kato's approach from 1958, a new extrapolation method based on the results of the database was developed. The mean squared error was reduced to 0.51.

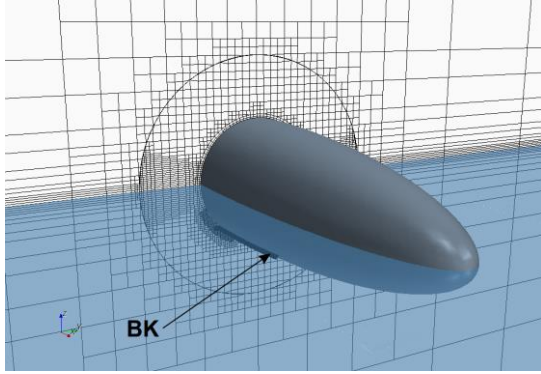


Figure 4: Simulation domain discretization for an ellipsoid body with free surface

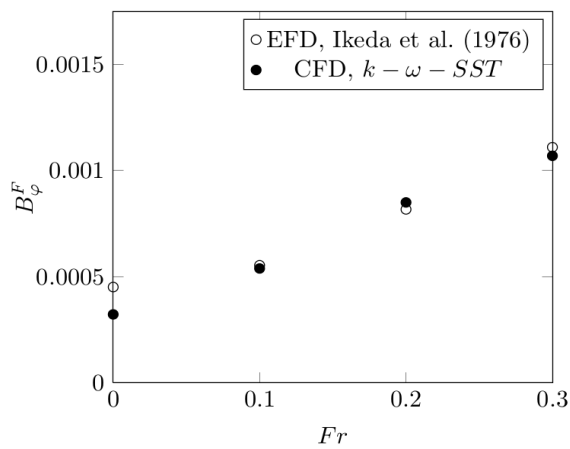


Figure 5: Frictional roll damping - comparison of experimental (Ikeda et al., 1976) and numerical results - rolling ellipsoid for various Froude numbers, grid resolution 1.3 Mio. cells, time step  $\Delta t = \pi/100\omega$

## 2. FVM SIMULATIONS

The simulation procedure is described in detail in Handschel et al. (2012, 2014). The solver STAR-CCM+ is used to simulate the incompressible flow around the rolling ship. The FVM solves the governing equations in integral form for mass and momentum, as well as for the volume fraction of water and air and equations for the turbulence modeling. The segregated iterative solution method is based on the SIMPLE-algorithm.

The computational domain is divided into two regions, see Figure 4. An inner cylinder (rotor) is rolling around a fixed roll axis. A sliding interface boundary condition is applied between the stationary (stator) and the rotating part of the grid. The grid is unstructured and trimmed hexahedral. A prism layer on the wall region exists. Local refinements are applied near the hull, the appendages and the free water surface. A volume of fluid (VOF) method is used to calculate the free

water surface flow. In all RANSE computations, the turbulence model  $k - \omega - SST$  is used. The dimensionless wall distance  $y^+$  for the first layer reaches values between 30 and 90.

Simulation results were compared with experimental results of an ellipsoid body, see Figure 4, measured by Ikeda (1976, Figure 5) and with results of the container ship Duisburg Test Case (DTC), see Handschel et al. (2014). The CFD results are in good agreement with the experiments.

To reduce simulation time, calculations with the ellipsoid body to estimate the normal forces on bilge keels were optimized. Instead of the previous described domain discretization, an ellipsoid with only one bilge keel is simulated. The rotor-stator motion model is replaced by complete mesh motion. The multi-phase flow is reduced to a single-flow simulation. For  $KC = 11.2$  a comparison was carried out. A deviation of 2% was achieved. The simulation time was further reduced by a splitting of the ellipsoid. Only half of the ellipsoid with the bilge keel was discretized. Results of the optimized CFD discretization have a good comparability to experimental results, see Figure 6.

## 3. NORMAL FORCES ON BILGE KEELS

To estimate normal forces on bilges keels, the moment  $M_{BK}$  around the longitudinal axis of the ellipsoid is determined by pressure integration. The moment can be formulated as Fourier polynomial:

$$M_{BK} = \sum_{j=1}^{\infty} [C_{A,j} \sin(j\omega t) + C_{B,j} \cos(j\omega t)]. \quad (6)$$

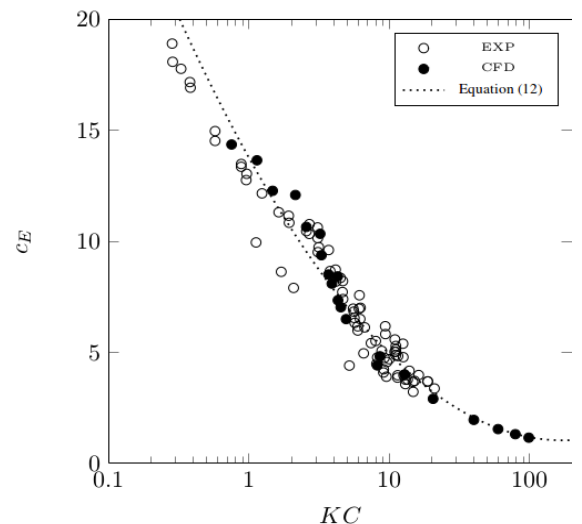


Figure 6: Force coefficients of normal forces on BK - Comparison of experimental values and CFD.

$C_{A,j}$  are coefficients in phase with the roll angle,  $C_{B,j}$  coefficients in phase with the roll velocity. Assuming harmonic roll motion behavior,

$$\varphi = \varphi_a \cdot \sin(\omega t), \quad (7)$$

the equivalent damping energy  $E_{BKe}$  can be expressed by the conservation of energy approach:

$$E_{BKe} = \pi \varphi_a C_{B,1}. \quad (8)$$

Details of this approach can be found in Wassermann et al. (2016). The moment  $M_{BK}$  can also be approximated by a force coefficient  $c_E$  approach with

$$M_{BK} = \frac{\rho}{2} c_E \omega^2 \varphi_a^2 \cos^2(\omega t) \int b_{BK} r_{BK}^3 dl \quad (9)$$

which leads to the energy over a roll cycle of

$$E_{BK} = \frac{4}{3} \rho c_E \omega^2 \varphi_a^3 \int b_{BK} r_{BK}^3 dl. \quad (10)$$

The relation  $E_{BKe} = E_{BK}$  results into an estimation approach for the force coefficient  $c_E$  of one bilge keel:

$$c_E = \frac{3\pi C_{B,1}}{4\rho\omega^2\varphi_a^2 \int b_{BK} r_{BK}^3 dl}. \quad (11)$$

The Fourier coefficient  $C_{B,1}$  is determined with a Fast Fourier Transformation (FFT) algorithm. All other parameters are simulation inputs.

In Figure 6, results of CFD simulations and the presented experiments of Figure 2 are compared. Simulation and experimental results are in very good agreement. The experimental and the simulation results can be approximated by:

$$c_E = 0.47 \cdot \ln(KC)^2 - 4.94 \cdot \ln(KC) + 13.75 \quad (12)$$

for  $0.3 < KC < 100$ .

Compared to Equation (1), the range of validity is significantly extended by Equation (12). Nevertheless, Equation (12) should be applied with care because a detailed validation study for the range of  $KC$ -numbers larger 20 is still missing. Simulations to estimate results for large  $KC$ -numbers are very sensitive to small changes in

simulation setups. As a precaution, it was decided to choose simulation setups for the approximation which achieve the smallest force coefficients.

#### 4. SKIN FRICTION ROLL DAMPING

Roll simulations with different roll setups for two ships in full scale, a RoPax (*m1413z006*, Handschel et al., 2012b) and a Pax (*m1399z001*) vessel, and simulations in model scale for the containership DTC (*m1398s001*, Handschel et al., 2014) were carried out to study skin friction roll damping. The main dimensions of the ship are listed in Table 2. The results were compared to Ikeda's method. The following differences could be observed:

1. The skin friction roll moment is not completely in phase with roll velocity. Based on measured phase angles  $\varepsilon_F$ , an averaged phase shift was determined:

$$\varepsilon_F = (-0.206 - \varepsilon_{F,BK}) \exp\left(\frac{U}{\sqrt{gL_{WL}}}\right) [rad]. \quad (13)$$

$\varepsilon_{F,BK} = 0$  for ships without,  $\varepsilon_{F,BK} = 0.18$  for ships with bilge keels.

2. The influence of forward speed on the skin friction roll moment is modeled by the ratio to the zero speed skin friction roll moment, see Equation (3). A comparison of this approach to simulation results is presented in Figure 7 (upper Figure). In the lower Figure, it can be clearly seen that the forward speed effect can be described more exactly by a formulation based on the ratio  $KC_L/\varphi_a$ . A correction of Tamiya's equation (3) to

$$\frac{M_{Fe}}{M_{F0e}} = 1 + 0.79 \frac{KC_L}{\varphi_a} - 0.022 \left(\frac{KC_L}{\varphi_a}\right)^2 \quad (14)$$

is recommended.

3. Kato used Hughes skin friction line as formulation for the skin friction force

| Dim.  | m1398s001 | m1399z001 | m1413z006 |
|-------|-----------|-----------|-----------|
| $L/B$ | 6.979     | 8.176     | 6.525     |
| $B/D$ | 4.246     | 4.456     | 4.304     |
| $L/D$ | 29.631    | 36.433    | 28.087    |
| $C_B$ | 0.632     | 0.647     | 0.542     |

Table 2: Main dimensions of the ships,  $L$ -ship length,  $B$ -ship breadth,  $D$ -ship draft,  $C_B$ -block coefficient

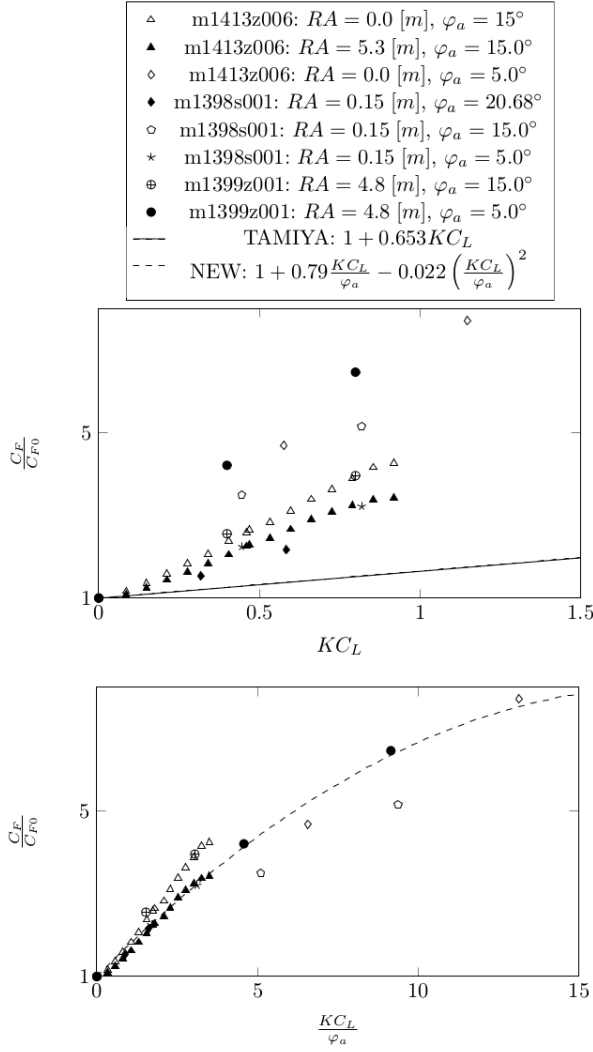


**Figure 7: Skin friction forward speed correction – Comparison Tamiya’s Equation (3) and new Equation (14) – RA - different roll axis heights**

coefficient. To consider the oscillating roll motion, the Reynolds number definition is modified. Based on experiments with small rolling cylinders, Kato estimated a correction factor  $k = 0.51$ . Although this factor could be confirmed for simulations in full scale, a factor of  $k = 2.5$  is recommended to consider the correct skin friction moment in model scale, see Table 3 of the Appendix. In Figure 8, it can be clearly seen that deviations of factor  $k$  have less influence on total roll damping for ships in full scale as for ships in model scale.

In the Appendix, Table 3 shows a comparison between simulations and the improved method as well as the original Ikeda method. The comparison is presented in two columns as a ratio of the maximum friction moment  $M_{F,max}$  for simulation

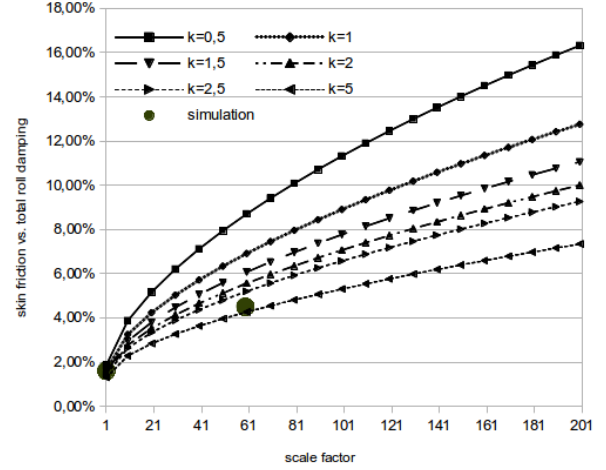


**Figure 8: Ratio of skin friction to total roll damping moment over  $\lambda$  for different correction factors  $k$**

results to the results of the new method, column (1), and Ikeda’s method, column (2):

$$\frac{M_{F,max,simulation}}{M_{F,max,methods}} \quad (15)$$

The new approach improves the mean squared error of Ikeda’s method from 1.75 to 0.51.

For a best-practice conversion approach of total roll damping,  $M(\dot{\phi}) = M_e \dot{\phi}$ , from model ( $m$ ) to full scale ( $FS$ ) with scale factor  $\lambda$ , the method can be applied as follows:

$$M_{e,FS} = \frac{\rho_{FS}}{\rho_m} M_{e,m} \lambda^2 - \quad (16)$$

$$\left[ \frac{1}{3\pi} \bar{r}_m^3 \varphi_a \omega_m S_m \lambda^2 (\rho_m C_{F,m} - \rho_{FS} C_{F,FS}) \cdot (-2 \sin(2\varepsilon_F) + \cos(2\varepsilon_F) + 3) \right]$$

$$C_F = C_{F0} \left[ 1 + 0.79 \frac{KC_L}{\varphi_a} - 0.022 \left( \frac{KC_L}{\varphi_a} \right)^2 \right] \quad (17)$$

$$KC_L = 2\pi \frac{U}{\omega L_{WL}} \quad for \ 0 < \frac{KC_L}{\varphi_a} < 20 \quad (18)$$

$$C_{F0} = 1.328 Re_{F,x}^{-0.5} + 0.016 Re_{F,x}^{-0.114} \quad (19)$$

$$Re_{F,m} = k \frac{\bar{r}_m^2 \varphi_a^2 \omega_m}{\nu_m} \quad and \quad Re_{F,FS} = k \frac{\bar{r}_{FS}^2 \varphi_a^2 \omega_{FS}}{\nu_{FS}} \quad (20)$$

with  $k = 2.5$

## 5. CONCLUSION

The investigation shows that the calculation of force coefficients based on Ikeda's method for normal forces on bilge keels and skin friction damping is not sufficient for today's application. Based on finite-volume method simulation results, an improved formulation for force coefficients of normal forces on bilge keels over a wider range of  $KC$  numbers could be determined, see Equation (12). To transfer the of the Reynolds number depending skin friction roll damping from model scale into full scale, an extrapolation method based on Kato's approach was developed. Especially for model tests with large scale factors, the best-practice conversion approach, Eq. (16-20), is advantageous. Nevertheless, a database with 39 simulations does not represent all types of ship forms and roll setups. To improve this approach, the database should be extended. Furthermore it should be noted that the presented simple parameter methods do not replace experiments or more exact simulation methods which should be preferred if possible.

## 6. ACKNOWLEDGEMENTS

The presented approximation methods were developed based on simulations which were carried out as part of a project which was funded by the German Federal Ministry of Economics and Technology under the aegis of the BMWi-project "Best-Rolldämpfung" within the framework program "Schiffahrt und Meerestechnik für das 21. Jahrhundert". The authors would like to thank the cooperation partners in the project: University Duisburg-Essen, SVA Potsdam and the DNV-GL.

## 7. REFERENCES

- 26th ITTC, Specialist Committee on Stability in Waves, 2011, "Recommended Procedures – Numerical Estimation of Roll Damping", International Towing Tank Conference, URL April 2016: <http://itc.info>.
- El Moctar, B., Shigunov, V. and Zorn, T., 2012, "Duisburg Test Case: Post-Panamax Containership for Benchmarking", Ship Technology Research / Schiffstechnik, Vol. 59/3.
- Fujino, M., Ida, T., Maeto, T., Numata, T., 1979, "A consideration on the hydrodynamic normal forces acting on bilge keel" (in Japanese), Jour. of KANSAI SNA, Vol. 144.
- Handsichel, S., Köllisch, N., Soproni, J.P., Abdel-Maksoud, M., 2012a, "A numerical method for estimation of ship roll damping for large amplitudes", 29<sup>th</sup> Symposium on Naval Hydrodynamics, Gothenburg, Sweden.
- Handsichel, S., Köllisch, N., Abdel-Maksoud, M., 2012b, "Roll Damping of Twin-Screw Vessels: Comparison of RANSE with Established Methods", Proceedings of the 11th International Conference on the Stability of Ships and Ocean Vehicles, Athens, Greece.
- Handsichel, S., Fröhlich, M., Abdel-Maksoud, M., 2014, "Experimental and Numerical Investigation of Ship Roll Damping by Applying the Harmonic Forced Roll Motion Technique", 30<sup>th</sup> Symposium on Naval Hydrodynamics, Hobart, Tasmania, Australia.
- Ikeda, Y., Himeno, Y., Tanaka, N., 1976, "Ship roll damping – frictional component and normal pressure on bilge keel" (in Japanese), Jour. of KANSAI SNA, Vol. 161.
- Ikeda, Y., Himeno, Y., Tanaka, N., 1978, "A Prediction Method for Ship Roll Damping", Report of the Department of Naval Architecture, University of Osaka Prefecture, No. 00405.
- Kato, H., 1958, "On the frictional resistance to the rolling ships" (in Japanese), Jour. of KANSAI SNA, Vol. 102.
- Komura, T. and Tamiya, S., 1972, "Topics on ship rolling characteristics with advance speed" (in Japanese), Jour. of KANSAI SNA, Vol. 132.
- Sarpkaya, T., O'Keefe, J.L., 1996, "Oscillating flow about two and three-dimensional bilge keels", Jour. of Offshore Mechanics and Artic, Vol. 1.
- Wassermann, S., Feder, D.-F., Abdel-Maksoud, M., 2016, "Estimation of Ship Roll Damping – a Comparison of the Decay and the Harmonic Excited Roll Motion Technique", Ocean Engineering Journal – Special Issues dedicated to Stability and Safety of Ships and Ocean Vehicles.

8. APPENDIX

| ship      | $\lambda$ | BK | $\varphi_a$ [°] | $T$ [s] | $RA$ [m] | $U$ [m/s] | $k$  | $\bar{r}$ [m] | $S$ [m <sup>2</sup> ] | (1)  | (2)  |
|-----------|-----------|----|-----------------|---------|----------|-----------|------|---------------|-----------------------|------|------|
| m1399z001 | 1.0       | x  | 5.0             | 9.5     | 4.8      | 5.40      | 0.51 | 12.40         | 9473.8                | 1.45 | 2.49 |
| m1399z001 | 1.0       | x  | 15.0            | 9.5     | 4.8      | 5.40      | 0.64 | 12.40         | 9473.8                | 1.27 | 1.47 |
| m1399z001 | 1.0       | x  | 25.0            | 9.5     | 4.8      | 5.40      | 2.67 | 12.40         | 9473.8                | 1.00 | 1.03 |
| m1399z001 | 1.0       | x  | 5.0             | 19.0    | 4.8      | 5.40      | 0.45 | 12.40         | 9473.8                | 1.55 | 3.53 |
| m1399z001 | 1.0       |    | 5.0             | 19.0    | 4.8      | 5.40      | 0.23 | 12.34         | 9343.6                | 1.89 | 4.29 |
| m1399z001 | 1.0       | x  | 15.0            | 19.0    | 4.8      | 5.40      | 0.42 | 12.40         | 9473.8                | 1.41 | 1.91 |
| m1399z001 | 1.0       |    | 15.0            | 19.0    | 4.8      | 5.40      | 0.12 | 12.34         | 9343.6                | 1.89 | 2.56 |
| m1399z001 | 1.0       | x  | 25.0            | 19.0    | 4.8      | 5.40      | 0.60 | 12.40         | 9473.8                | 1.26 | 1.44 |
| m1399z001 | 1.0       |    | 25.0            | 19.0    | 4.8      | 5.40      | 0.11 | 12.34         | 9343.6                | 1.78 | 2.00 |
| m1399z001 | 1.0       | x  | 5.0             | 38.0    | 4.8      | 5.40      | 0.36 | 12.40         | 9473.8                | 1.74 | 4.88 |
| m1399z001 | 1.0       |    | 5.0             | 38.0    | 4.8      | 5.40      | 0.26 | 12.34         | 9343.6                | 1.94 | 5.44 |
| m1399z001 | 1.0       | x  | 15.0            | 38.0    | 4.8      | 5.40      | 0.34 | 12.40         | 9473.8                | 1.53 | 2.47 |
| m1399z001 | 1.0       |    | 15.0            | 38.0    | 4.8      | 5.40      | 0.13 | 12.34         | 9343.6                | 1.97 | 3.18 |
| m1399z001 | 1.0       | x  | 25.0            | 38.0    | 4.8      | 5.40      | 0.34 | 12.40         | 9473.8                | 1.46 | 1.85 |
| m1399z001 | 1.0       |    | 25.0            | 38.0    | 4.8      | 5.40      | 0.09 | 12.34         | 9343.6                | 1.99 | 2.51 |
| m1399z001 | 1.0       | x  | 5.0             | 9.5     | 0.0      | 5.40      | 0.72 | 9.67          | 9473.8                | 1.35 | 2.24 |
| m1399z001 | 1.0       | x  | 15.0            | 9.5     | 0.0      | 5.40      | 0.71 | 9.67          | 9473.8                | 1.26 | 1.42 |
| m1399z001 | 1.0       | x  | 25.0            | 9.5     | 0.0      | 5.40      | 4.00 | 9.67          | 9473.8                | 0.93 | 0.94 |
| m1399z001 | 1.0       | x  | 5.0             | 19.0    | 0.0      | 5.40      | 0.75 | 9.67          | 9473.8                | 1.38 | 3.01 |
| m1399z001 | 1.0       | x  | 15.0            | 19.0    | 0.0      | 5.40      | 0.83 | 9.67          | 9473.8                | 1.24 | 1.64 |
| m1399z001 | 1.0       | x  | 25.0            | 19.0    | 0.0      | 5.40      | 1.09 | 9.67          | 9473.8                | 1.15 | 1.28 |
| m1399z001 | 1.0       | x  | 5.0             | 38.0    | 0.0      | 5.40      | 0.50 | 9.67          | 9473.8                | 1.62 | 4.37 |
| m1399z001 | 1.0       | x  | 15.0            | 38.0    | 0.0      | 5.40      | 0.46 | 9.67          | 9473.8                | 1.46 | 2.29 |
| m1399z001 | 1.0       | x  | 25.0            | 38.0    | 0.0      | 5.40      | 0.45 | 9.67          | 9473.8                | 1.40 | 1.73 |
| m1398s001 | 59.5      | x  | 4.9             | 2.49    | 0.15     | 1.47      | 5.85 | 0.352         | 5.585                 | 0.71 | 1.44 |
| m1398s001 | 59.5      | x  | 12.8            | 2.49    | 0.15     | 1.47      | 2.44 | 0.352         | 5.585                 | 1.01 | 1.22 |
| m1398s001 | 59.5      | x  | 4.9             | 3.49    | 0.15     | 0.0       | 3.27 | 0.352         | 5.585                 | 0.89 | 0.46 |
| m1398s001 | 59.5      | x  | 19.6            | 3.49    | 0.15     | 0.0       | 1.98 | 0.352         | 5.585                 | 1.08 | 0.64 |
| m1398s001 | 59.5      | x  | 4.9             | 2.22    | 0.15     | 0.0       | 2.82 | 0.352         | 5.585                 | 0.95 | 0.50 |
| m1398s001 | 59.5      | x  | 14.8            | 2.22    | 0.15     | 0.0       | 1.84 | 0.352         | 5.585                 | 1.11 | 0.65 |
| m1413z006 | 1.0       | x  | 5.0             | 14.6    | 5.3      | 0.0       | 0.43 | 10.38         | 4678.0                | 1.57 | 1.12 |
| m1413z006 | 1.0       | x  | 15.0            | 14.6    | 5.3      | 0.0       | 0.64 | 10.38         | 4678.0                | 1.29 | 1.05 |
| m1413z006 | 1.0       | x  | 25.0            | 14.6    | 5.3      | 0.0       | 0.45 | 10.38         | 4678.0                | 1.34 | 1.14 |
| m1413z006 | 1.0       | x  | 5.0             | 14.6    | 5.3      | 5.53      | 0.45 | 10.38         | 4678.0                | 1.56 | 3.81 |
| m1413z006 | 1.0       | x  | 15.0            | 14.6    | 5.3      | 5.53      | 0.46 | 10.38         | 4678.0                | 1.38 | 1.98 |
| m1413z006 | 1.0       | x  | 25.0            | 14.6    | 5.3      | 5.53      | 0.73 | 10.38         | 4678.0                | 1.22 | 1.43 |
| m1413z006 | 1.0       | x  | 5.0             | 14.6    | 5.3      | 11.06     | 0.44 | 10.38         | 4678.0                | 1.57 | 4.78 |
| m1413z006 | 1.0       | x  | 15.0            | 14.6    | 5.3      | 11.06     | 0.29 | 10.38         | 4678.0                | 1.53 | 2.70 |
| m1413z006 | 1.0       | x  | 25.0            | 14.6    | 5.3      | 11.06     | 0.26 | 10.38         | 4678.0                | 1.48 | 2.00 |

Table 3: Skin friction roll damping moment – Comparison new method (1) and Ikeda’s method (2)

